# Bohmian quantum trajectories from coherent states

**Sanjib Dey and Andreas Fring**

*Department of Mathematical Science, City University London, Northampton Square, London EC1V 0HB, UK*
*E-mail: sanjib.dey.1@city.ac.uk, a.fring@city.ac.uk*

Abstract: We find that real and complex Bohmian quantum trajectories resulting from well-localized Klauder coherent states in the quasi-Poissonian regime possess qualitatively the same type of trajectories as those obtained from a purely classical analysis of the corresponding Hamilton-Jacobi equation. In the complex cases treated the quantum potential results to a constant, such that the agreement is exact. For the real cases we provide conjectures for analytical solutions for the trajectories as well as the corresponding quantum potentials. The overall qualitative behaviour is governed by the Mandel parameter determining the regime in which the wavefuntions evolve as soliton like structures. We demonstrate these features explicitly for the harmonic oscillator and the Pöschl-Teller potential.

## 1. Introduction

Bohmian mechanics was originally proposed sixty years ago [1] to address some of the difficulties present in the standard formulation of quantum mechanics based on the Copenhagen interpretation and its aim was to provide an alternative ontological view. Its central purpose is to avoid the need for the collapse of the wavefunction and instead provide a trajectory based scheme allowing for a causal interpretation. While this metaphysical discussion is still ongoing and is in parts very controversial [2, 3, 4], it needs to be stressed that Bohmian mechanics leads to the same predictions of measurable quantities as the orthodox framework. Here we will leave the interpretational issues aside and build on the fact that the Bohmian formulation of quantum mechanics has undoubtedly proven to be a successful technical tool for the study of some concrete physical scenarios. For instance, it has been applied successfully to study of photodissociation problems [5], tunneling processes [6], atom diffraction by surfaces [7, 8, 9] and high harmonic generation [10]. Whereas these applications are mainly based on an analysis of real valued quantum trajectories, more recently there has also been the suggestion [11, 12] for a formulation of Bohmian mechanics based on complex trajectories. We will discuss here both versions, but it is this latter formulation on which we will place our main focus and which will be the main subject of our investigations in this manuscript.

Independently from the above suggestions, an alternative perspective on complex classical mechanics has recently emerged out of the study of complex quantum mechanical Hamiltonians. It is by now well accepted that a large class of such systems constitute well-defined self-consistent descriptions of physical systems [13, 14, 15] with real energy eigenvalue spectra and unitary time-evolution. The dynamics of many classical models has been investigated, for instance complex extensions of standard one particle systems [16, 17, 18], non-Hamiltonian dynamical systems [19], chaotic systems [20] or deformations of many-particle systems such as Calogero-Moser-Sutherland models [21, 22, 23, 24]. From those studies conclusions were drawn for example with regard to tunneling behaviour [18] or the existence of band structures [25]. It was also shown [26] that complex solutions to a large class of complex quantum mechanical systems arise as special cases from the study of Korteweg-deVries type of field equations, see [27] for a review on new models obtained from deformations of integrable systems.

It is therefore natural to compare these two formulations and address the question of whether they are equivalent in some regime. We will demonstrate here that this is indeed the case, since the complex Bohmian quantum mechanics based on so-called Klauder coherent states [28, 29, 30, 31] in the quasi-Poissonian regime is identical to a purely classical study of the Hamilton-Jacobi equations.

Our manuscript is organized as follows: In section two we recall the basic equations of Bohmian mechanics in the real as well as the complex case together with the main features of Klauder coherent states. In section 3 we compare in both cases the trajectories resulting from standard Gaussian wavepackets and those resulting from Klauder coherent states with a purely classical treatment. For the latter case we verify the validity of a conjectured formula for the trajectories. In section 4 we discuss the same scenario for the Pöschl-Teller potential. Our conclusions are stated in section 5

## 2. Real and complex Bohmian mechanics, Klauder coherent states

Let us briefly recall the key equations of Bohmian mechanics for reference purposes and also to establish our conventions and notations. The starting point for the construction of the Bohmian quantum trajectories is usually a solution of the time-dependent Schrödinger equation involving a potential $V(x)$

$$i\hbar\frac{\partial\psi(x,t)}{\partial t} = -\frac{\hbar^2}{2m}\frac{\partial^2\psi(x,t)}{\partial x^2} + V(x)\psi(x,t). \tag{2.1}$$

The two variants leading either to real or complex trajectories are distinguished by different parameterizations of the wavefunctions.

### 2.1 The real variant

The version based on real valued trajectories results from the WKB-polar decomposition

$$\psi(x,t) = R(x,t)e^{i/\hbar S(x,t)}, \qquad \text{with} \quad R(x,t), S(x,t) \in \mathbb{R}. \tag{2.2}$$

Upon the substitution of (2.2) into (2.1) the real and imaginary part are identified as

$$S_t + \frac{(S_x)^2}{2m} + V(x) - \frac{\hbar^2}{2m}\frac{R_{xx}}{R} = 0, \qquad \text{and} \qquad mR_t + R_x S_x + \frac{1}{2}RS_{xx} = 0, \tag{2.3}$$

usually referred to as the quantum Hamilton-Jacobi equation and the continuity equation, respectively. When considering these equations from a classical point of view, the second term in the first equation of (2.3) is interpreted as the kinetic energy such that the real velocity $v(t)$ and the last term, the so-called quantum potential $Q(x,t)$, result to

$$mv(x,t) = S_x = \frac{\hbar}{2i}\left[\frac{\psi^*\psi_x - \psi\psi_x^*}{\psi^*\psi}\right], \quad Q(x,t) = -\frac{\hbar^2}{2m}\frac{R_{xx}}{R} = \frac{\hbar^2}{4m}\left[\frac{(\psi^*\psi)_x^2}{2\left(\psi^*\psi\right)^2} - \frac{(\psi^*\psi)_{xx}}{\psi^*\psi}\right], \tag{2.4}$$

respectively. The corresponding time-dependent effective potential is therefore $V_{\text{eff}}(x,t) = V(x) + Q(x,t)$. Then one has two options to compute quantum trajectories. One can either solve directly the first equation in (2.4) for $x(t)$ or employ the effective potential $V_{\text{eff}}$ solving $m\ddot{x} = -\partial V_{\text{eff}}/\partial x$ instead. Due to the different order of the differential equations to be solved, we have then either one or two free parameter available. Thus for the two possibilities to coincide the initial momentum is usually not free of choice, but the initial position $x(t=0) = x_0$ is the only further input. The connection to the standard quantum mechanical description is then achieved by computing expectation values from an ensemble of $n$ trajectories, e.g. $\langle x(t)\rangle_n = 1/n \sum_{i=1}^{n} x_i(t)$.

### 2.2 The complex variant

In contrast, the version based on complex trajectories is computed from a parameterization of the form

$$\psi(x,t) = e^{i/\hbar \tilde{S}(x,t)}, \qquad \text{with } \tilde{S}(x,t) \in \mathbb{C}. \tag{2.5}$$

The substitution of (2.5) into (2.1) yields the single equation

$$\tilde{S}_t + \frac{(\tilde{S}_x)^2}{2m} + V(x) - \frac{i\hbar}{2m}\tilde{S}_{xx} = 0. \tag{2.6}$$

Interpreting this equation in a similar way as in the previous subsection, but now as a complex quantum Hamilton-Jacobi equation, the second term in (2.6) yields a complex velocity and the last term becomes a complex quantum potential

$$m\tilde{v}(x,t) = \hat{S}_x = \frac{\hbar}{i}\frac{\psi_x}{\psi}, \quad \tilde{Q}(x,t) = -\frac{i\hbar}{2m}\tilde{S}_{xx} = -\frac{\hbar^2}{2m}\left[\frac{\psi_{xx}}{\psi} - \frac{\psi_x^2}{\psi^2}\right]. \tag{2.7}$$

The corresponding time-dependent effective potential is now $\tilde{V}_{\text{eff}}(x,t) = V(x) + \tilde{Q}(x,t)$. Once again one has two options to compute quantum trajectories, either solving the first equation in (2.7) for $x(t)$, which is, however, now a complex variable. Alternatively, we may also view the effective Hamiltonian $H_{\text{eff}} = p^2/2m + \tilde{V}_{\text{eff}}(x,t) = H_r + iH_i$ in its own right and simply compute the equations of motion directly from

$$\dot{x}_r = \frac{1}{2}\left(\frac{\partial H_r}{\partial p_r} + \frac{\partial H_i}{\partial p_i}\right), \qquad \dot{x}_i = \frac{1}{2}\left(\frac{\partial H_i}{\partial p_r} - \frac{\partial H_r}{\partial p_i}\right), \tag{2.8}$$

$$\dot{p}_r = -\frac{1}{2}\left(\frac{\partial H_r}{\partial x_r} + \frac{\partial H_i}{\partial x_i}\right), \qquad \dot{p}_i = \frac{1}{2}\left(\frac{\partial H_r}{\partial x_i} - \frac{\partial H_i}{\partial x_r}\right), \tag{2.9}$$

where we use the notations $x = x_r + ix_i$ and $p = p_r + ip_i$ with $x_r$, $x_i$, $p_r$, $p_i \in \mathbb{R}$. For the complex case the relation to the conventional quantum mechanical picture is less well established although some versions have been suggested to extract real expectation values, e.g. based on taking time-averaged mean values [32], seeking for isochrones [33, 34] or using imaginary part of the velocity field of particles on the real axis [35].

We will here evaluate the expressions for the velocity, the quantum potential and the resulting trajectories for two solvable potentials commencing with different choices of solutions $\psi$. Our particular focus is here on commencing from coherent states and for that reason we state their main properties.

### 2.3 Klauder coherent states

For Hermitian Hamiltonians $\mathcal{H}$, with discrete bounded below and nondegenerate eigenspectrum $E_n = \omega e_n$ and orthonormal eigenstates $|\phi_n\rangle$ the Klauder coherent states [28, 29, 30, 31] are defined in general as

$$\psi_J(x,t) := \frac{1}{\mathcal{N}(J)} \sum_{n=0}^{\infty} \frac{J^{n/2} \exp(-i\omega t e_n)}{\sqrt{\rho_n}} \phi_n(x), \qquad J \in \mathbb{R}_0^+. \tag{2.10}$$

The probability distribution and the normalization constant are given by $\rho_n := \prod_{k=1}^{n} e_k$ and $\mathcal{N}^2(J) := \sum_{k=0}^{\infty} J^k/\rho_k$, respectively. To allow for a more compact notation we adopt the usual convention $\rho_0 = 1$ throughout the manuscript. The key properties of these states are their continuity in time and the variable $J$, the fact that they provide a resolution of the identity and that they are temporarily stable satisfying the action angle identity $\langle J, \omega t| \mathcal{H} |J, \omega t\rangle = \hbar\omega J$.

Evidently the expression for $\psi_J(x,t)$ is only meaningful when the wave packet is properly localized, i.e. the absolute value squared of the weighting function $c_n(J) = J^{n/2}/\mathcal{N}(J)\sqrt{\rho_n}$ needs to be peaked about some mean value $\langle n\rangle = 2Jd\ln\mathcal{N}(J)/dJ$. The deviation from a Poissonian distribution is captured in the so-called Mandel parameter [36] defined as

$$Q := \frac{\Delta n^2}{\langle n\rangle} - 1 = J\frac{d}{dJ}\ln\frac{d}{dJ}\ln\mathcal{N}^2(J), \tag{2.11}$$

with dispersion $\Delta n^2 = \langle n^2\rangle - \langle n\rangle^2$. Here the case $Q = 0$ is a pure Poisson distribution with $Q < 0$ and $Q > 0$ corresponding to sub-Poisson and super-Poisson distributions, respectively. We refer to distributions with $|Q| \ll 1$ as quasi-Poissonian.

## 3. The harmonic oscillator

The harmonic oscillator

$$\mathcal{H}_{\rm ho} = \frac{p^2}{2m} + \frac{1}{2}m\omega^2 x^2, \tag{3.1}$$

constitutes a very instructive example on which many of the basic features can be understood. We will therefore take it as a starting point. Many results may already be found in the literature, but for completeness we also report them here together with some new findings.

### 3.1 Real case

As reported for instance by Holland [3], using the two formulae in (2.4) it is easy to see that for any stationary state $\psi_n(x,t) = \phi_n(x)e^{-iE_nt/\hbar}$, with $\phi_n(x)$ being a solution of the stationary Schrödinger, the velocity in (2.4) results to $v(t) = 0$. This is compatible with the values obtained from the use of the quantum potential $Q(x) = E_n - V(x)$, because this corresponds to a classical motion in a constant effective potential $V_{\text{eff}}(x,t) = E_n$. This is of course qualitatively very far removed from our original potential (3.1), such that classical trajectories obtained from $\mathcal{H}_{\text{ho}}$ and its effective version are fundamentally of qualitatively different nature.

Instead we would expect, that when starting from coherent states we end up with a behaviour much closer to the classical behaviour resulting from the original Hamiltonian. By direct computation shown in [3], using the standard Gaussian wavepackets of the form

$$\psi_c(x,t) = \left(\frac{m\omega}{\hbar\pi}\right)^{1/4} e^{-\frac{m\omega}{2\hbar}(x-a\cos\omega t)^2 - \frac{i}{2}\left[\omega t + \frac{m\omega}{\hbar}\left(2xa\sin\omega t - \frac{1}{2}a^2\sin 2\omega t\right)\right]}, \tag{3.2}$$

to compute the above quantities with $a$ being the centre of the wavepacket at $t = 0$, one obtains from (2.4) equations for the velocity and the quantum potential as

$$v(x,t) = -a\omega\sin\omega t, \qquad \text{and} \qquad Q(x,t) = \frac{\hbar\omega}{2} - \frac{1}{2}m\omega^2(x - a\cos\omega t)^2. \tag{3.3}$$

Solving now the first equation in (3.3) with $dx/dt = v(x,t)$ for $x(t) = a(\cos\omega t - 1) + x_0$ with initial condition $x(0) = x_0$, we may construct the corresponding potential from $m\ddot{x} = -\partial V/\partial x$. The result is compatible with the effective potential obtained from $Q(x,t)+V(x)$ when replacing the explicit time dependent terms with expressions in $x(t)$. Alternatively, from the effective potential

$$V_{\text{eff}}[x(t)] = \frac{1}{2}m\omega^2(x(t) - x_0 - a)^2 + \frac{\hbar\omega}{2}, \tag{3.4}$$

Newton's equation will give the above solution for $x(t)$. Thus for the states $\psi_c(x,t)$ the Bohmian trajectories for the harmonic oscillator potential $\mathcal{H}_{\text{ho}}$ are indeed the same as those resulting from the motion in a classical harmonic oscillator potential.

What has not been analyzed this far is the use the more general Klauder coherent states (2.10) as input into the evaluation of the Bohmian trajectories and corresponding quantum potential $Q(x,t)$. Since we have $e_n = n$ for the case at hand, the probability distribution and normalization constant are computed to $\rho_n = n!$ and $\mathcal{N}(J) = e^{J/2}$, respectively. The solution for the stationary Schrödinger equation is well known to be the normalized wavefunction $\phi_n(x) = (\frac{m\omega}{\pi\hbar})^{1/4}\exp\left(-\frac{mx^2\omega}{2\hbar}\right)H_n\left(x/\sqrt{\frac{\hbar}{m\omega}}\right)/\sqrt{2^n n!}$ with $H_n(x)$ denoting Hermite polynomials. The Mandel parameter $Q$ in (2.11) always equals zero independently of $J$, such that we are always dealing with a Poissonian distribution.

Due to the fact that $\psi_J(x,t)$ involves an infinite sum, it is complicated to compute analytic expressions for the quantities in (3.3). However, since we expect a close resemblance to the expressions obtained from standard coherent states $\psi_c(x,t)$, we suggest here that

the corresponding Bohmian trajectories and quantum potential are given by

$$x(t) = x^J_{\max}(\cos\omega t - 1) + x_0 \qquad \text{and} \qquad Q(x,t) = \frac{\hbar\omega}{2} - \frac{1}{2}m\omega^2(x - x^J_{\max}\cos\omega t)^2, \quad (3.5)$$

respectively. Our conjecture is guided by the analogy to the previous case, $x^J_{\max}$ is taken here to be the centre of the wavepacket, i.e. $x^J_{\max} = \max|\psi_J(x,0)|$. In this case we compute the quantities of interest numerically[1]. We observe stability for $\psi_J(x,t)$ computed from (2.10) up to six digits, when terminating the sum at $n = 150$. Our results for the trajectories and quantum potential are depicted in figure 1(a) and 1(b), respectively.

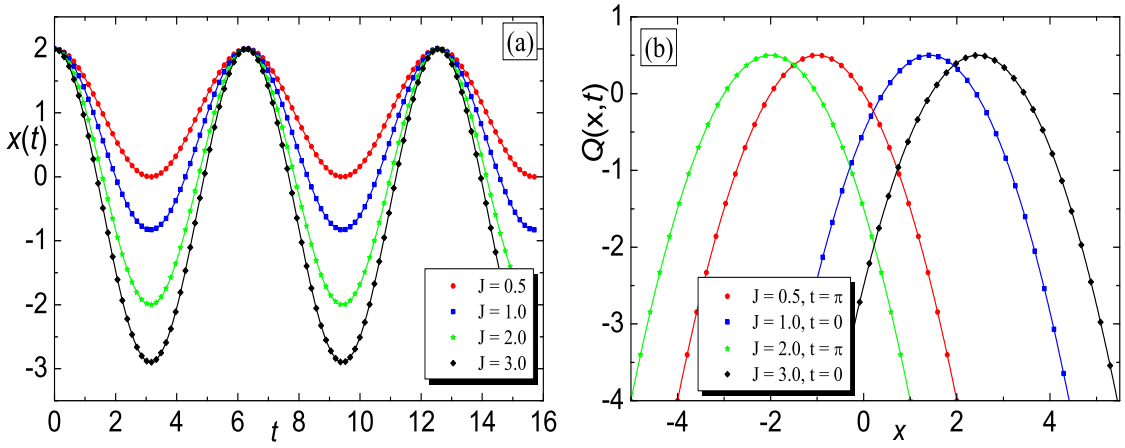


**Figure 1:** (Color online) (a) Real Bohmian quantum trajectories as functions of time from Klauder coherent states (scattered) versus classical trajectories corresponding to (3.5) (solid lines). (b) Quantum potential from Klauder coherent states (scattered) versus conjectured formula (3.5) (solid lines). We have taken $x_0 = 2$ and computed the maxima to $x^{0.5}_{\max} = 1$, $x^1_{\max} = 1.4142$, $x^2_{\max} = 2$, $x^3_{\max} = 2.4495$. (In au.)

We observe perfect agreement between the numerical computation of $x(t)$ from solving the first equation in (2.4) using the expression (2.10) for the Klauder coherent states for various values of $J$ and the conjectured analytical expression (3.5) for $x(t)$ in which we only compute the value for $x^J_{\max}$ numerically. We find a similar agreement for the computation of the quantum potential $Q(x,t)$, either numerically using the expression (2.10) in the second equation in (2.4) or from the conjectured analytical expression in (3.5). We also find agreement between the two computations solving either directly the first equation in (2.4) for $x(t)$ or employing the effective potential $V_{\text{eff}}$ to solve $m\ddot{x} = -\partial V_{\text{eff}}/\partial x$ instead. What remains is the interesting challenge to compute the infinite sums together with the subsequent expressions explicitly in an analytical manner.

### 3.2 Complex case

As in the previous subsection we start again with stationary states $\psi_n(x,t) = \phi_n(x)e^{-iE_nt/\hbar}$ as basic input into our computation as outlined in subsection 2.2. A fundamental difference

[1] We always use atomic units (au), taking $\omega = 1$, $\hbar = 1$ and $m = 1$ in all numerical computations throughout the manuscript.

to the real case is that now we do not obtain a universal answer for all models. From (2.7) we compute

$$\tilde{v}_0(x,t) = i\omega x, \qquad \tilde{Q}_0(x,t) = \frac{\hbar\omega}{2}, \tag{3.6}$$

$$\tilde{v}_1(x,t) = i\omega x - \frac{i\hbar}{mx}, \qquad \tilde{Q}_1(x,t) = \frac{\hbar\omega}{2} + \frac{\hbar^2}{2mx^2}. \tag{3.7}$$

As discussed in [37], for $n = 1, 2$ the explicit analytical solutions may be found in these cases. By direct integration of the first equations in (3.6), (3.7) or from $m\ddot{x} = -\partial V_{\text{eff}}/\partial x$ we compute

$$x_0(t) = x_0 e^{i\omega t}, \quad \text{and} \quad x_1(t) = \pm\sqrt{\frac{\hbar}{m\omega} + e^{2it\omega}\left(x_0^2 - \frac{\hbar}{m\omega}\right)}. \tag{3.8}$$

For larger values of $n$ we obtain more complicated equations for the velocities and quantum potentials, which may be solved numerically for $x(t)$, see also [37, 38]. For instance, we obtain from (2.7)

$$\tilde{v}_5(x,t) = ix\omega - \frac{5i\hbar}{mx} + \frac{60i\hbar^3 - 40i\hbar^2 mx^2\omega}{15\hbar^2 mx - 20\hbar m^2x^3\omega + 4m^3x^5\omega^2}, \tag{3.9}$$

$$\tilde{Q}_5(x,t) = \frac{\hbar\left(225\hbar^5 + 225\hbar^4 mx^2\omega + 200\hbar^2m^3x^6\omega^3 - 80\hbar m^4x^8\omega^4 + 16m^5x^{10}\omega^5\right)}{2m\left(15\hbar^2x - 20\hbar mx^3\omega + 4m^2x^5\omega^2\right)^2} \tag{3.10}$$

The solutions for $x_1(t)$ and $x_5(t)$ are depicted in figure 2.

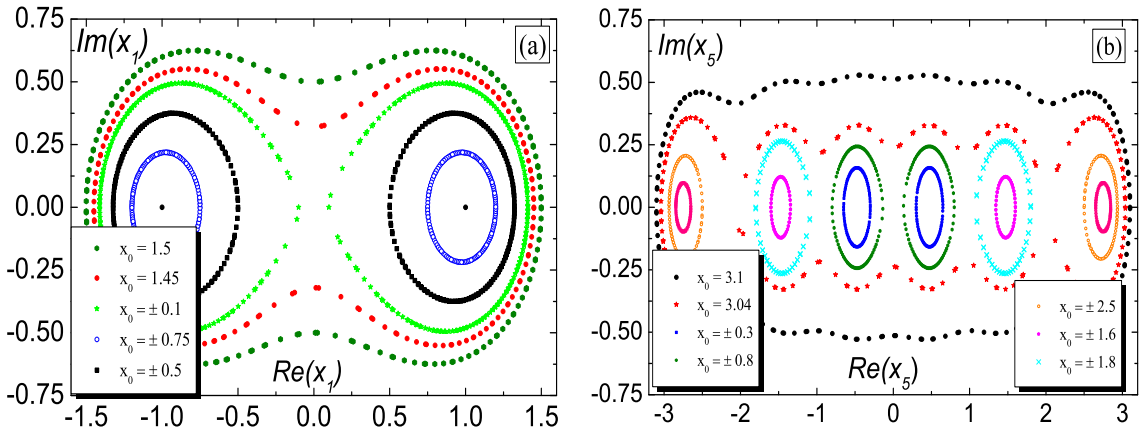


**Figure 2:** (Color online) Complex Bohmian quantum trajectories as functions of time for different initial values $x_0$ resulting from stationary states $\psi_1(x,t)$ and $\psi_5(x,t)$ in panel (a) and (b), repectively. (In au.)

In both cases we observe that the fixed points, at $\pm 1$ for $\tilde{v}_1(x,t)$ and at $\pm 0.476251$, $\pm 1.47524$, $\pm 2.75624$ for $\tilde{v}_5(x,t)$, are centres surrounded by closed limit cycles. For large enough initial values we also observe bounded motion surrounding all fixed points.

Next we use once more the Gaussian wavepackets (3.2) as input to evaluate the velocity and the quantum potential from (2.7)

$$\tilde{v}(x,t) = -\omega(x_i + a\sin\omega t) + i\omega(x_r - a\cos\omega t), \qquad \text{and} \qquad \tilde{Q}(x,t) = \frac{\hbar\omega}{2}, \tag{3.11}$$

The value for the constant quantum potential was also found in [34]. Solving now the equation of motion with $\tilde{v}(t)$ for $x_r$ and $x_i$ we obtain a complex trajectory

$$x(t) = \left(\frac{a}{2} + c_1\right)\cos\omega t - c_2\sin\omega t + i\left[c_2\cos\omega t + \left(c_1 - \frac{a}{2}\right)\sin\omega t\right], \tag{3.12}$$

with integration constants $c_1$ and $c_2$. We compare this with the classical result computed from the complex effective Hamiltonian

$$\mathcal{H}_{\text{eff}} = \frac{1}{2m}(p_r^2 - p_i^2) + \frac{m\omega^2}{2}(x_r^2 - x_i^2) + i\left(\frac{1}{m}p_r p_i + m\omega^2 x_r x_i\right) + \frac{\hbar\omega}{2}. \tag{3.13}$$

We may think of this Hamiltonian as being $\mathcal{PT}$-symmetric, where the symmetry is induced by the complexification and realized as $\mathcal{PT}$: $x_r \to -x_r$, $x_i \to x_i$, $p_r \to p_r$, $p_i \to -p_i$, $i \to -i$. The equations of motion are then computed according to (2.8) and (2.9) to

$$\dot{x}_r = \frac{p_r}{m}, \quad \dot{x}_i = \frac{p_i}{m}, \quad \dot{p}_r = -m\omega^2 x_r, \quad \text{and} \quad \dot{p}_i = -m\omega^2 x_i. \tag{3.14}$$

As these equations decouple, they are easily solved. We find

$$x(t) = x_r(0)\cos\omega t + \frac{p_r(0)}{m\omega}\sin\omega t + i\left[x_i(0)\cos\omega t + \frac{p_i(0)}{m\omega}\sin\omega t\right]. \tag{3.15}$$

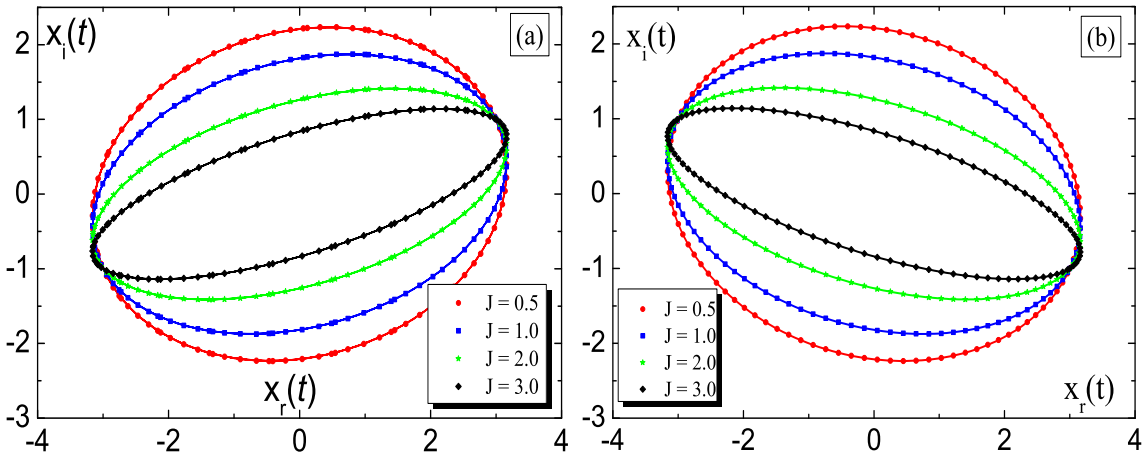


**Figure 3:** (Color online) Complex Bohmian trajectories resulting from Klauder coherent states (scattered) compared to the purely classical computation (3.15) (solid) for different values of $J$, with initial value (a) $x_0 = 3 + i$ and (b) $x_0 = 3 - i$ with maximal values $x^{0.5}_{\max} = 1$, $x^{1}_{\max} = 1.4142$, $x^{2}_{\max} = 2$, $x^{3}_{\max} = 2.4495$. (In au.)

In order to compare this now with the outcome from taking general Klauder coherent states (2.10) in the evaluation of $\tilde{v}(t)$ and $\tilde{Q}(x,t)$ and the corresponding trajectories we

require the four initial values. In contrast, solving the first order differential equation for the velocity (2.7) we only require the two initial values for the complex position. To compute the initial values for the momentum we can take again the results for the Gaussian wavepackets as a guide and compare (3.12) and (3.15). The compatibility between the two then requires

$$x_r(0) = \frac{p_i(0)}{m\omega} + x^J_{\max}, \qquad \text{and} \qquad x_i(0) = -\frac{p_r(0)}{m\omega}, \tag{3.16}$$

where we have replaced $a$ by $x^J_{\max}$. We can now either simply solve this for the initial values for the momentum (3.16) or alternatively use directly the same initial values obtained from the solution of (2.7). Comparing the direct parametric plot of (3.15) for the stated initial conditions with the numerical computation of the complex Bohmian trajectories resulting from Klauder coherent states, we find perfect agreement as depicted in figure 3.

Thus under these constraints for the initial conditions the trajectories resulting from a classical analysis of the effective Hamiltonian (3.13) and the integration of the complex Bohmian trajectories resulting from Klauder coherent states are identical. Notice that the quantum nature of $\mathcal{H}_{\text{eff}}$ is only visible in form of the overall constant $\hbar\omega/2$, which does, however, not play any role in the computation of the equations of motion.

## 4. The Pöschl-Teller potential

Next we discuss the Bohmian trajectories associated with the Pöschl-Teller Hamiltonian [39] of the form

$$\mathcal{H}_{\text{PT}} = \frac{p^2}{2m} + \frac{V_0}{2}\left[\frac{\lambda(\lambda-1)}{\cos^2(x/2a)} + \frac{\kappa(\kappa-1)}{\sin^2(x/2a)}\right] - \frac{V_0}{2}(\lambda+\kappa)^2 \quad \text{for } 0 \leq x \leq a\pi, \tag{4.1}$$

with $V_0 = \hbar^2/(4ma^2)$. This model has been widely discussed in the mathematical physics literature, e.g. [40, 31], since it has the virtue of being exactly solvable, classically as well as quantum mechanically. For a given energy $E$ a classical solution is known to be

$$x(t) = a \arccos\left[\frac{\alpha-\beta}{2} + \sqrt{\gamma}\cos\left(\sqrt{\frac{2E}{m}}\frac{t}{a}\right)\right], \tag{4.2}$$

with $\alpha = \lambda(\lambda-1)V_0/E$, $\beta = \kappa(\kappa-1)V_0/E$ and $\gamma = \alpha^2/4 + \beta^2/4 - \alpha\beta/2 - \alpha - \beta + 1$. The time dependent Schrödinger equation is solved by discrete eigenfunctions

$$\psi_n(x,t) = \frac{1}{\sqrt{N_n}}\cos^\lambda\left(\frac{x}{2a}\right)\sin^\kappa\left(\frac{x}{2a}\right)\ {}_2F_1\left[-n, n+\kappa+\lambda; k+\frac{1}{2}; \sin^2\left(\frac{x}{2a}\right)\right] e^{-iE_nt/\hbar} \tag{4.3}$$

with ${}_2F_1$ denoting the Gauss hypergeometric function. The corresponding energy eigenvalues and the normalization factor are given by

$$E_n = \frac{\hbar^2}{2ma^2}n(n+\kappa+\lambda), \quad N_n = a2^n n!\frac{\Gamma(\kappa+1/2)\Gamma(n+\lambda+1/2)}{\Gamma(2n+1+\lambda+\kappa)}\prod_{l=1}^{n}\frac{n-1+l+\kappa+\lambda}{2l-1+2\kappa}, \tag{4.4}$$

respectively. We will use these solutions in what follows.

### 4.1 Real case

As in the previous case we start with the construction of the trajectories from stationary states (4.3). Once again for the real case the computation is unspectacular in this case since the velocity computed from (2.4) is $v(t) = 0$ and the corresponding quantum potential results again simply to $Q(x) = E_n - V_{\mathrm{PT}}(x)$, such that classical trajectories correspond to a motion in a constant effective potential $V_{\mathrm{eff}}(x,t) = E_n$.

More interesting, and qualitatively very close to the classical behaviour, are the trajectories resulting from the Klauder coherent states given by the general expression (2.10). In this case the probability distribution is computed with $e_n = n(n+\kappa+\lambda)$ to $\rho_n = n!(n+\kappa+\lambda)_n$, where $(x)_n := \Gamma(x+n)/\Gamma(x)$ denotes the Pochhammer symbol. With these expressions the normalization constant results to a confluent hypergeometric function $\mathcal{N}^2(J) = {}_0F_1\left(1+\kappa+\lambda; J\right)$, from which we compute the Mandel parameter (2.11) to

$$Q(J,\kappa+\lambda) = \frac{J}{2+\kappa+\lambda}\,\frac{{}_0F_1\left(3+\kappa+\lambda; J\right)}{{}_0F_1\left(2+\kappa+\lambda; J\right)} - \frac{J}{1+\kappa+\lambda}\,\frac{{}_0F_1\left(2+\kappa+\lambda; J\right)}{{}_0F_1\left(1+\kappa+\lambda; J\right)}\,. \tag{4.5}$$

Using the relation between the confluent hypergeometric function and the modified Bessel function this is easily converted into the expression found in [31]. We agree with the finding therein that $Q$ is always negative, but disagree with the statement that $Q$ tends to zero for large $J$ for fixed $\kappa$, $\lambda$. Instead we argue that for fixed coupling constants the Mandel parameter $Q$ is a monotonically decreasing function of $J$ with $Q(0,\kappa+\lambda) = 0$. Assuming that the coherent states closely resemble a classical behaviour, we conjecture here in analogy to the classical solution (4.2) that the quantum trajectories acquire the general form

$$x(t) = a\arccos\left[\frac{X_+}{2} + \frac{X_-}{2}\cos\left(2\pi\frac{t}{T}\right)\right], \tag{4.6}$$

with $X_\pm = \cos(x_0/a) \pm \cos(x_m/a)$, $T$ denoting the period and $x_m = x(T/2) = \max[x(t)]$. Our conjecture is based on an extrapolation of the analysis of the relations between $\alpha$ and $\beta$ and functions of $x(0)$ and $x(T/2)$. The effective potential computed from (4.6) is then of Pöschl-Teller type

$$V_{\mathrm{eff}} = \frac{2ma^2\pi^2}{T^2}\left[\frac{\cos^2(x_0/2a)\cos^2(x_m/2a)}{\cos^2(x/2a)} + \frac{\sin^2(x_0/2a)\sin^2(x_m/2a)}{\sin^2(x/2a)}\right]. \tag{4.7}$$

As in the previous case we will compute the quantum trajectories numerically[2]. Our results from solving (2.4) are depicted in figure 4.

Most importantly we observe that the behaviour of the trajectories is entirely controlled by the values of the Mandel parameter $Q$. Panel (a) and (b) show trajectories for different values of $J$ with pairwise identical values of the Mandel parameter, that is $Q(2,190) = Q(0.0022906,5) = -0.000054529$, $Q(0.5,190) = Q(0.00057265,5) = -0.000013634$ and $Q(0.1,190) = Q(0.000114531,5) = -2.72691\times10^{-6}$. We notice that the overall qualitative behaviour is simply rescaled in time. We further observe a small deviation from

[2] We take $a = 2$ in all numerical computations in this section.

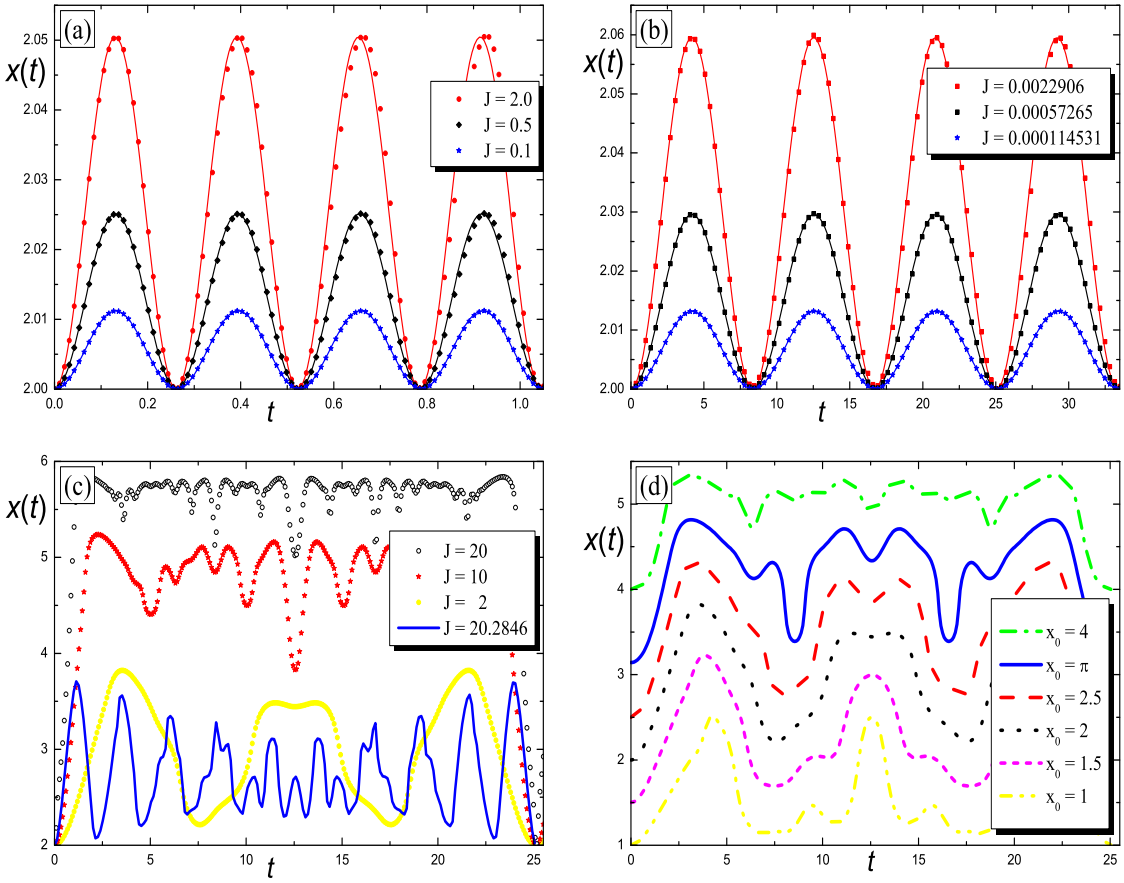


**Figure 4:** (Color online) Real Bohmian trajectories as functions of time from Klauder coherent states (scattered) versus classical trajectories (solid lines) corresponding to (4.6). (a) Quasi-Poissonian distribution with initial value $x_0 = 2$, coupling constants $\kappa = 90$, $\lambda = 100$, maxima $x_{\rm m}^2 = 2.0504447$, $x_{\rm m}^{0.5} = 2.0251224$, $x_{\rm m}^{0.1} = 2.0112100$ and periods $T^2 = 0.2612875$, $T^{0.5} = 0.2622200$, $T^{0.1} = 0.2627495$ for different values of $J$. (b) Quasi-Poissonian distribution with initial value $x_0 = 2$, coupling constants $\kappa = 2$, $\lambda = 3$, maxima $x_{\rm m}^{0.0022906} = 2.059522$, $x_{\rm m}^{0.00057265} = 2.0295876$, $x_{\rm m}^{0.000114531} = 2.0131884$ and periods $T^{0.0022906} = 8.34795$, $T^{0.00057265} = 8.36305$, $T^{0.000114531} = 8.37129$ for different values of $J$. (c) Sub-Poissonian distribution with initial value $x_0 = 2$, coupling constants $\kappa = 2$, $\lambda = 3$ for $J = 2, 10, 20$ (scattered) and $\kappa = 9$, $\lambda = 10$ for $J = 20.2846$ (solid). (d) Sub-Poissonian distribution for various initial values with coupling constants $\kappa = 2$, $\lambda = 3$ for $J = 2$. (In au.)

the periodicity growing with increasing time. As a consequence the matching between the quantum trajectories obtained from solving (2.4) and our conjectured analytical expression (4.6) is good for small values of time, but worsens as time increases. The agreement improves the closer the Mandel parameter approaches the Poissonian distribution, i.e. $Q = 0$. Once the Mandel parameter becomes very negative the correlation between the classical motion and the Bohmian trajectories is entirely lost as shown in panel (c) of figure 4 for $Q(2, 5) = -0.0425545$, $Q(10, 5) = -0.149523$ and $Q(20, 5) = -0.218944$. We also notice from panel (c) that the qualitative similarity observed for equal values of the Mandel para-

meter seen in panels (a) and (b) is lost once the states do not resemble a classical behaviour. This is seen by comparing the yellow dotted line and the solid blue line corresponding to the same values $Q(2,5) = Q(20.2846,19) = -0.0425545$. Panel (d) shows the sensitivity with regard to the initial values $x_0$. Whereas for the trajectories resembling the classical motion (4.6) this change does not affect the overall qualitative behaviour, it produces a more significant variation in the non-classical regime.

The explanation for this behaviour is that in the quasi-Poissonian regime the coherent states evolve as soliton like structures keeping their shape carrying out a periodic motion in time. In contrast, in the sub-Poissonian regime the motion is no longer periodic and the initial Gaussian shape of the wave is dramatically changed under the evolution of time. These features are demonstrated in figure 5.

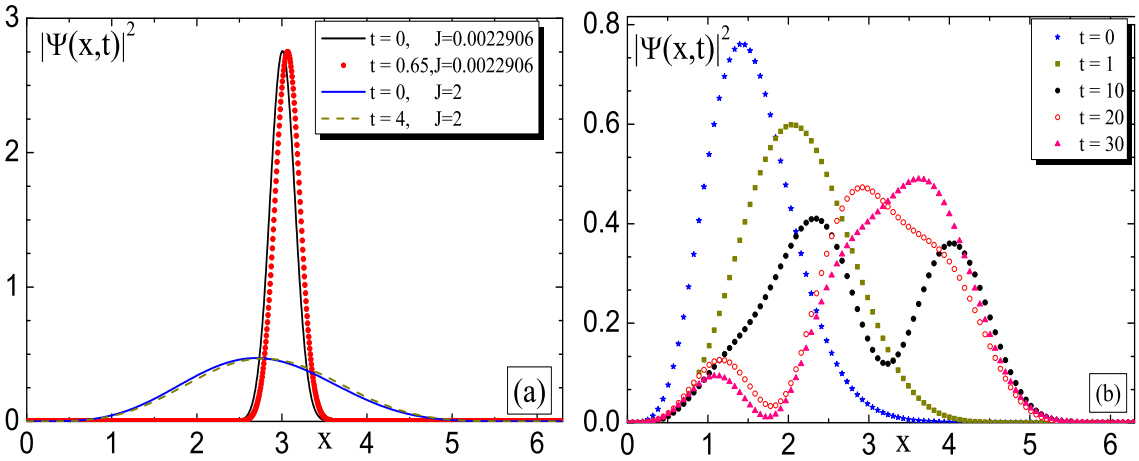


**Figure 5:** (Color online) (a) Periodic soliton like motion in the quasi-Poissonian regime for $\kappa = 90$, $\lambda = 100$ (thin) and $\kappa = 2$, $\lambda = 3$ (broad) with $Q = -0.000054529$ identical in both cases. (b) Spreading wave in the sub-Poissonian regime with $Q = -0.0917752$ for $J = 5$ and $\kappa = 2$, $\lambda = 3$. (In au.)

In figure 6 we plot the uncertainty relations for comparison.

In panel (a) we observe that in the quasi-Poissonian regime the saturation level is almost reached with $\Delta x \Delta p$ being very close to $\hbar/2$, oscillating around 0.5106 with a deviation of $\pm 0.0006$ and in the subpanel oscillating around 0.5000065 with a deviation of $\pm 0.0000008$. This is of course compatible with the very narrow soliton like structure observed in figure 5 leading to a classical type of behaviour. However, in the sub-Poissonian regime the uncertainty becomes larger, as seen in panel (b), corresponding to a spread out wave behaving very non-classical.

### 4.2 Complex case

Let us now consider the complex Bohmian trajectories starting once again with the construction from stationary states $\psi_n(x,t) = \phi_n(x)e^{-iE_n t/\hbar}$. For the lowest states we may

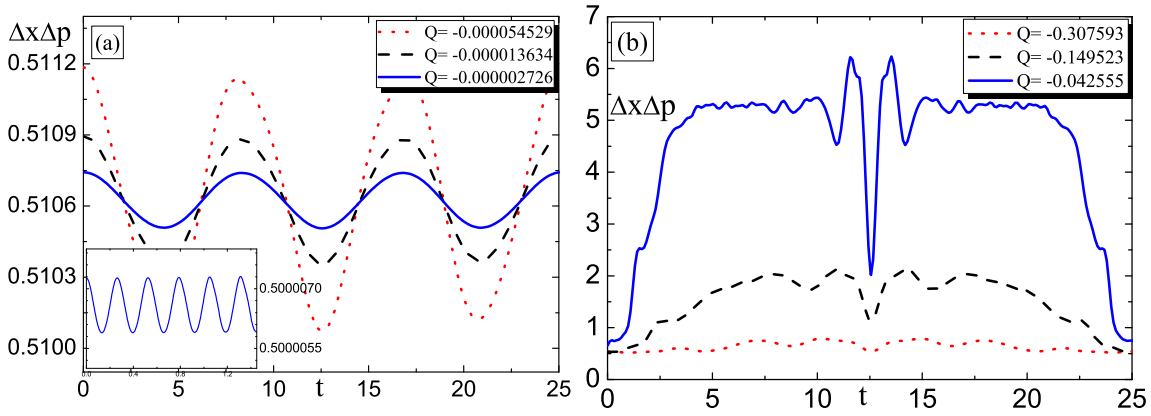


**Figure 6:** (Color online) Product of the position and momentum uncertainty as functions of time for different values of the Mandel parameter $Q$. (a) The coupling constants are $\kappa = 2, \lambda = 3$, with $J = 0.0022906$ (red dotted), $J = 0.00057265$ (black dashed), $J = 0.000114531$ (blue solid) and $J = 0.1$ for the subpanel with $\kappa = 90, \lambda = 100$. (b) The coupling constants are $\kappa = 2, \lambda = 3$ with $J = 2$ (red dotted), $J = 10$ (black dashed) and $J = 50$ (blue solid). (In au.)

compute analytical expressions from (2.7) for the velocities

$$\tilde{v}_0(x,t) = \frac{\hbar\left[(\kappa+\lambda)\cos\left(\frac{x}{a}\right)+\kappa-\lambda\right]}{i2am\sin\left(\frac{x}{a}\right)}, \tag{4.8}$$

$$\tilde{v}_1(x,t) = \frac{\hbar\left[(2\kappa^2+\kappa)\cot\left(\frac{x}{2a}\right)+(2\lambda^2+\lambda)\tan\left(\frac{x}{2a}\right)-(\kappa+\lambda+1)(\kappa+\lambda+2)\sin\left(\frac{x}{a}\right)\right]}{i2am\left[(\kappa+\lambda+1)\cos\left(\frac{x}{a}\right)+\kappa-\lambda\right]},$$

and the quantum potentials

$$\tilde{Q}_0(x,t) = V_0\frac{\left[(\kappa-\lambda)\cos\left(\frac{x}{a}\right)+\kappa+\lambda\right]}{\sin^2\left(\frac{x}{a}\right)}, \tag{4.9}$$

$$\tilde{Q}_1(x,t) = \frac{V_0}{2}\left[\frac{4(\kappa+\lambda+1)\left((\kappa-\lambda)\cos\left(\frac{x}{a}\right)+\kappa+\lambda+1\right)}{\left[(\kappa+\lambda+1)\cos\left(\frac{x}{a}\right)+\kappa-\lambda\right]^2}+\frac{\kappa}{\sin^2\left(\frac{x}{2a}\right)}+\frac{\lambda}{\cos^2\left(\frac{x}{2a}\right)}\right].$$

We note that the quantum potential $\tilde{Q}_1(x,t)$ resembles a Pöschl-Teller potential apart from its first term. For $n = 0$ we solve (2.7) analytically for the trajectories

$$x_0(t) = \pm a\arccos\left\{\frac{\left[(\kappa+\lambda)\cos\left(\frac{x_0}{a}\right)+\kappa-\lambda\right]e^{\frac{iht(\kappa+\lambda)}{2a^2m}}+\lambda-\kappa}{\kappa+\lambda}\right\}. \tag{4.10}$$

For excited states one may easily solve these equations numerically as depicted in figure 7.

We observe the usual appearance of the only possible types of fixed points in a Hamiltonian system, that is centres and saddle points. For the ground state we observe a close resemblance of the qualitative behaviour with the solution of the first excited state obtained for the harmonic oscillator as shown in figure 2.

Unlike the trajectories resulting from coherent states those obtained from stationary states are not expected to have a similar behaviour to the purely classical ones obtained

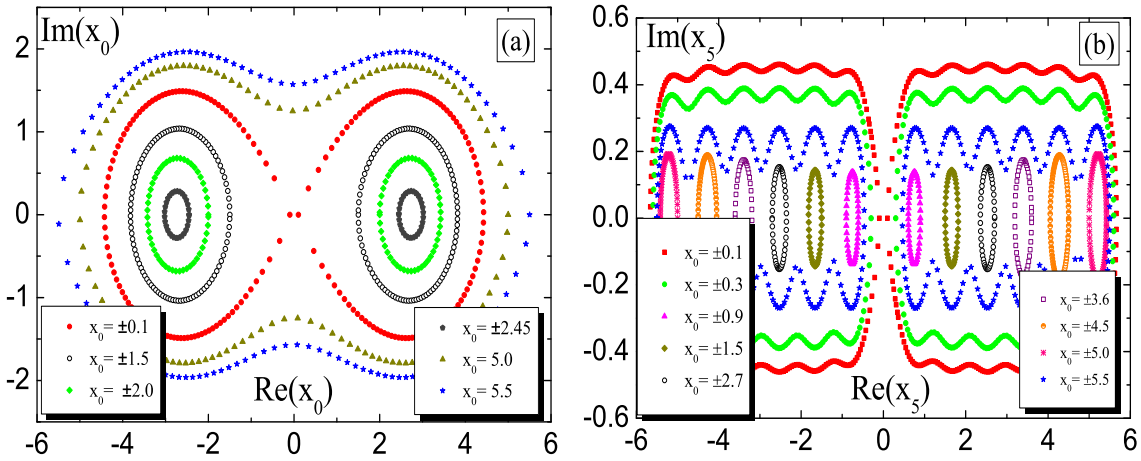


**Figure 7:** (Color online) Complex Bohmian trajectories as functions of time for different initial values $x_0$ resulting from stationary states $\Psi_0(x,t)$ and $\Psi_5(x,t)$ in panel (a) and (b), respectively. (In au.)

from solving directly the equations of motion (2.8) and (2.9). Complexifying the variables as specified after (2.8) and (2.9), we may split the Hamiltonian into its real and imaginary part $\mathcal{H}_{\rm PT} = H_r + iH_i$ with

$$H_r = \frac{p_r^2 - p_i^2}{2m} + V_0 \left[ \frac{(\lambda^2-\lambda)\left[\cosh\left(\frac{x_i}{a}\right)\cos\left(\frac{x_r}{a}\right)+1\right]}{\left[\cosh\left(\frac{x_i}{a}\right)+\cos\left(\frac{x_r}{a}\right)\right]^2} - \frac{(\kappa^2-\kappa)\left[\cosh\left(\frac{x_i}{a}\right)\cos\left(\frac{x_r}{a}\right)-1\right]}{\left[\cos\left(\frac{x_r}{a}\right)-\cosh\left(\frac{x_i}{a}\right)\right]^2} \right]$$
$$-\frac{V_0}{2}(\lambda+\kappa)^2,$$
$$H_i = \frac{p_i p_r}{m} + V_0 \left[ \frac{(\lambda^2-\lambda)\sinh\left(\frac{x_i}{a}\right)\sin\left(\frac{x_r}{a}\right)}{\left[\cosh\left(\frac{x_i}{a}\right)+\cos\left(\frac{x_r}{a}\right)\right]^2} - \frac{(\kappa^2-\kappa)\sinh\left(\frac{x_i}{a}\right)\sin\left(\frac{x_r}{a}\right)}{\left[\cos\left(\frac{x_r}{a}\right)-\cosh\left(\frac{x_i}{a}\right)\right]^2} \right]. \tag{4.11}$$

This Hamiltonian also respects the aforementioned $\mathcal{PT}$-symmetry $\mathcal{PT}$: $x_r \to -x_r$, $x_i \to x_i$, $p_r \to p_r$, $p_i \to -p_i$, $i \to -i$. Contourplots of the potential are shown in figures 9 and 10 with the colourcode convention being associated to the spectrum of light decreasing from red to violet. The corresponding equations of motion are easily computed from (2.8) and (2.9), albeit not reported here as they are very lengthy, and solved numerically as shown for some parameter choices in the figures 8, 9 and 10 as solid lines.

Let us now compare them with the complex Bohmian trajectories computed from the Klauder coherent states (2.10). A previous initial attempt to compute these trajectories has been made in [41], however, the preliminary computations presented there do not agree with our findings. We start by depicting a case for the quasi-Poissonian distribution in figure 8.

Remarkably, in that case we find a perfect match between these two entirely different computations. We observe that unlike as for the real trajectories, for which we required an effective potential to achieve agreement, these computations are carried out in both cases for exactly the same coupling constants $\kappa$ and $\lambda$ with no adjustments made. Thus, just as for the harmonic oscillator, this suggests that the complex quantum potential is simply

a constant such that the effective potential essentially coincides with the original one in (4.1). From the trajectories with larger radii in panel (a) we observe that the trajectories do not close and are not perfect ellipses. Prolonging the time beyond the cut-off time in the panel (a) scenario we find inwardly spiralling trajectories. The coincidence between the purely classical calculation and the quantum trajectories still persists for larger values of $J$ and more asymmetrical initial conditions closer to the boundary of the potential as shown for an example in panel (b). For larger values of time we encounter numerical problems due to the poor convergence of the series for large values of $J$.

Our initial values in 8(a) are chosen to lie on the isochrones, that is the set of all points which when evolved in time will arrive all simultaneously, say at $t_f$, on the real axis. The isochrone is indicated in figure 8(a) by a red line and an additional arrow attached to it pointing in the direction in which the real axis is reached. In our example the arrival time is chosen to be $t = 0.04$. As discussed for instance in [33, 34] the wavefunction defined on the isoclines can be thought of as leading to physical information as their corresponding complex quantum trajectories acquire real values. Moreover, as shown in [34], one may even reconstruct the precise form of the entire wavefunction from the knowledge of the isochrone and the information transported by the action. We will follow up this line of enquiry elsewhere.

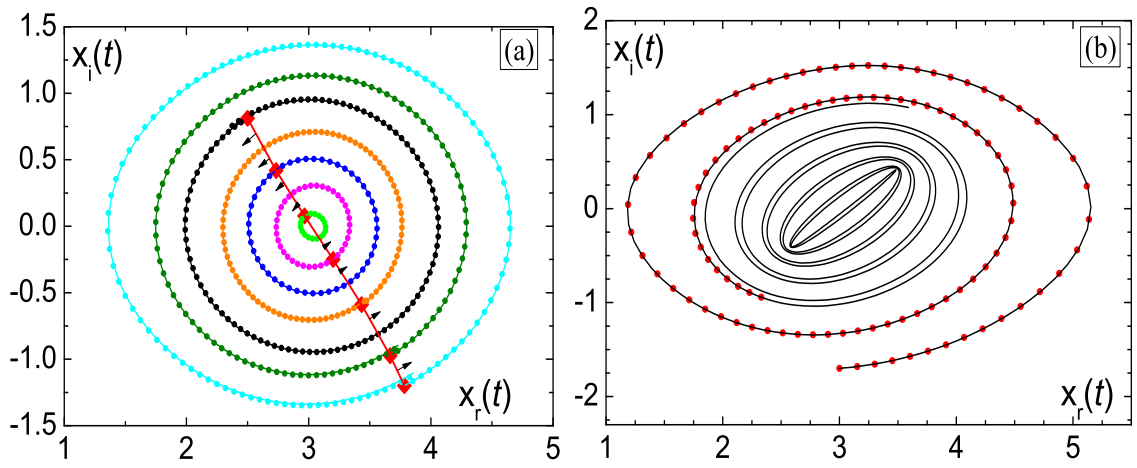


**Figure 8:** (Color online) Complex Bohmian trajectories as functions of time from Klauder coherent states (scattered) versus classical trajectories corresponding to solutions of (2.8) and (2.9) for the complex Pöschl-Teller Hamiltonian $\mathcal{H}_{\rm PT}$ (4.11) (solid lines) for quasi-Poissonian distribution with $\kappa = 90$, $\lambda = 100$. (a) The evolution is shown from $t = 0$ to $t = 0.27$ with initial values on the isochrone with $t_f = 0.04$ for $J = 0.5$ and in (b) from $t = 0$ to $t = 0.5$ (quantum) and $t = 0$ to $t = 3.0$ (classical) with initial value $x_0 = 3 - 1.7i$ and $p_0 = 32.907 + 3.16416i$ for $J = 20$. The energy for this trajectory is therefore $E = \mathcal{H}_{\rm PT}(x_0, p_0) = -8.44045 + 102.134i$. (In au.)

The qualitative behaviour of the classical trajectories can be understood by considering the motion in the complex potential. We consider first a trajectory of a particle with real energy depicted in figure 9 as ellipse.

The initial position is taken to be on the real axis with the particle getting a kick parallel to the imaginary axis. Within the real part of the potential the particle starts on

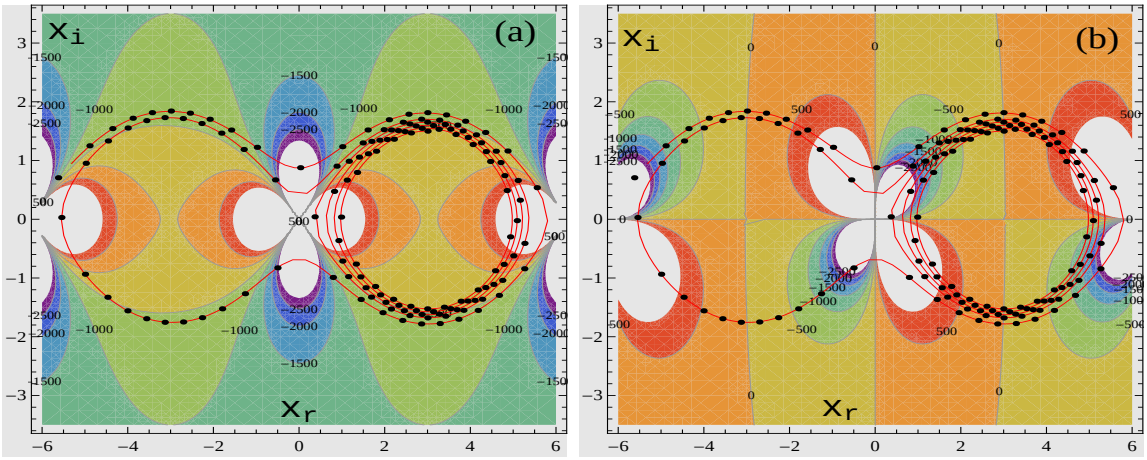


**Figure 9:** (Color online) Complex Bohmian quantum trajectories as functions of time from $J = 0.5$-Klauder coherent states (scattered) versus classical trajectories (solid lines) corresponding to solutions of (2.8) and (2.9) for the complex Pöschl-Teller potential $V_{\mathrm{PT}}$ (a) real part, (b) imaginary part for quasi-Poissonian and localized distribution from $t = 0$ to $t = 1.78$ with $\kappa = 90$, $\lambda = 100$. The initial values are $x_0 = 3 + 1.5i$, $p_0 = -30.1922 + 0.385121i$ such that $E = -6.55991 - 13.5182i$ (black solid, red scattered) and $x_0 = 4.5$, $p_0 = 41.8376i$ with real energy $E = -31.7564$ (blue solid, red scattered). (In au.)

a higher potential level and would simply role down further up into the upper half plane towards the imaginary axis due to the curvature of the potential. However, the particle is also subjected to the influence of the imaginary part of the potential and at roughly $x_r = 3$ this effect is felt when the particle reaches a turning point, pulling it back to the real axis which is reached at the point when reflecting $x_i$ at the turning point. At that point it has reached a higher potential level from which it roles down back to the initial position through the lower half plane in a motion similar to the one performed in the upper half plane.

Trajectories with complex values for the initial values have in general also complex energies. As can be seen in figure 9 for a specific case, we obtain at first a qualitatively similar motion to the real case, with the difference that the particle spirals outwards. In the real part of the potential this has the effect that after a few turns the particle is eventually attracted by the sink on top of the origin. The momentum it gains through this effect propels it into the region with negative real part. Thus the particle has bypassed the infinite potential barrier at the origin on the real axis, tunneling to the next potential minimum, i.e. to the forbidden region in the real scenario. Similar effects have been observed in the purely classical treatment of a complex elliptic potential in [18]. The continuation of this trajectory and scenarios for other parameter choices can be understood in a similar manner. For instance in figure 10 we depict a trajectory which does not spiral at first, but the particle has instead already enough momentum that allows it to tunnel directly into the negative region.

As in the real scenario the Mandel parameter controls the overall qualitative behaviour, although in the complex case this worsens for non-real initial values that is complex

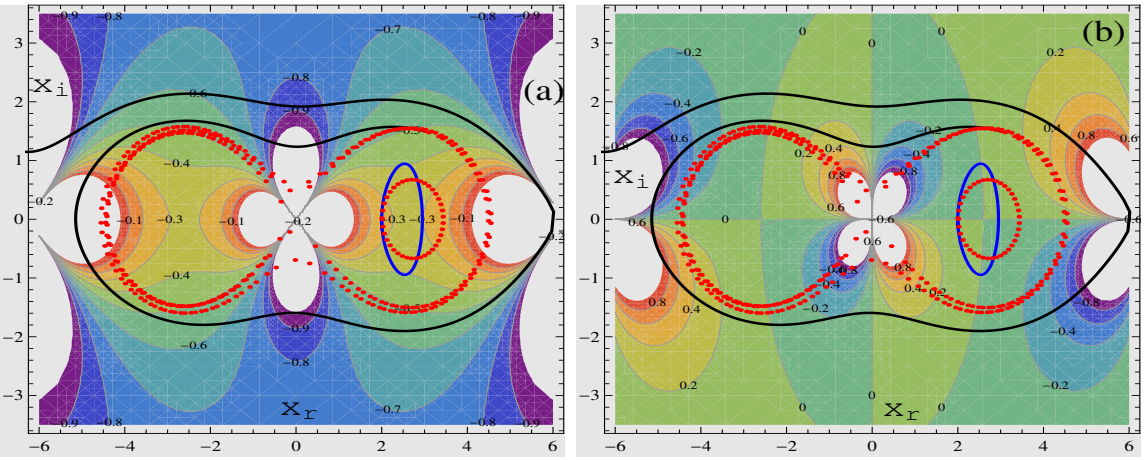


**Figure 10:** (Color online) Complex Bohmian trajectories as functions of time from $J = 0.00057265$-Klauder coherent states (scattered) versus classical (solid lines) corresponding to solutions of (2.8) and (2.9) for the complex Pöschl-Teller potential $V_{\mathrm{PT}}$ (a) real part, (b) imaginary part for the quasi-Poissonian regime and spead distribution from $t = 0$ to $t = 100$ (quantum) and $t = 0$ to $t = 32$ (classical) with $\kappa = 2$, $\lambda = 3$. The initial values are $x_0 = 3 + 1.5i$ and $p_0 = -0.788329 + 0.157336i$ such that $E = -0.187539 - 0.0275087i$ (black solid, red scattered) and $x_0 = 2$, $p_0 = -0.49446i$ with real energy $E = -0.277833$ (blue solid, red scattered). (In au.)

energies. In quasi-Poissonian regime pictured in figure 8 and 9 we observe a complete match between the purely classical and the quantum computation. However, this agreement ceases to exist in figure 10, despite the fact that it is showing a quasi-Poissonian case with the same value for $Q$. The difference is that in the latter case the wavefunction is less well localized as we saw in figure 5. As can be seen in figure 10, for real energies we still have the same qualitative behaviour, but for complex energies the less localized wave is spread across a wide range of potential levels such that it can no longer mimic the same classical motion. However, qualitatively we can see that in principle it is still compatible with the motion in a complex classical Pöschl-Teller potential.

As can be seen in figure 11 this resemblances ceases to exist when we enter the sub-Poissonian regime.

We observe that the correlation between the two behaviours is now entirely lost. Notably, the quantum trajectories enter into regions not accessible to the classical ones. However, in a very coarse sense we can still explain the overall behaviour of the quantum trajectories by appealing to the complex potential.

## 5. Conclusions

We have computed real and complex quantum trajectories in two alternative ways, either by solving the associated equation for the velocity or by solving the Hamilton-Jacobi equations taking the quantum potential as a starting point. In all cases considered we found perfect agreement for the same initial values in the position.

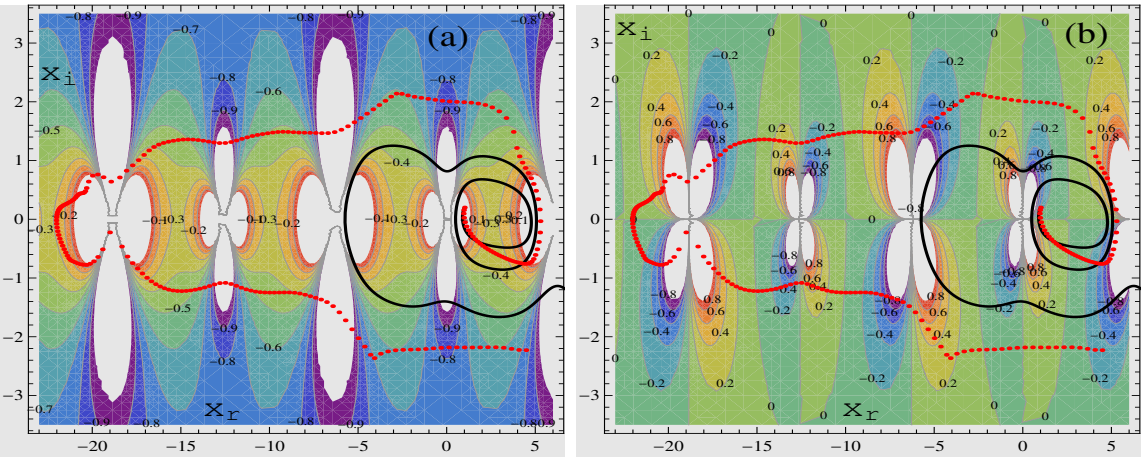


**Figure 11:** (Color online) Complex Bohmian trajectories as functions of time from $J = 10$-Klauder coherent states (scattered) versus classical (solid lines) corresponding to solutions of (2.8) and (2.9) for the complex Pöschl-Teller potential $V_{\rm PT}$ (a) real part, (b) imaginary part for the sub-Poissonian regime from $t = 0$ to $t = 21$ (quantum) and $t = 0$ to $t = 32$ (classical) with $\kappa = 2$, $\lambda = 3$. The initial values are $x_0 = 2 + 0.2i$ and $p_0 = -0.665052 - 0.406733i$ such that $E = -0.0941366 - 0.364635i$ (black solid, red scattered). (In au.)

Our main concern in this manuscript has been to investigate the quality of the Klauder coherent states and test how close they can mimic a purely classical description. This line of enquiry continues our previous investigations [42, 43] for these type of states in a different context. We have demonstrated that in the quasi-Poissonian regime well localized Klauder coherent states produce the same qualitative behaviour as a purely classical analysis. We found these features in the real as well as in the complex scenario. For the real trajectories we conjectured some analytical expressions reproducing the numerically obtained results. Whereas the real case required always some adjustments, we found for the complex analysis of the harmonic oscillator and the Pöschl-Teller potential a precise match with the purely classical treatment.

Naturally there are a number of open problems left: Clearly it would be interesting to produce more sample computations for different types of potentials, especially for the less well explored complex case. In that case it would also be very interesting to explore further how the conventional quantum mechanical description can be reproduced. Since Bohmian quantum trajectories allow to establish that link there would be no need to guess any rules in the classical picture mimicking some quantum behaviour as done in the literature.

**Acknowledgments:** SD is supported by a City University Research Fellowship. AF thanks C. Figueira de Morisson Faria for useful discussions.

## References

[1] D. Bohm, A Suggested interpretation of the quantum theory in terms of hidden variables. 1., Phys. Rev. **85**, 166–179 (1952).

[2] B. Bohm and B. Hiley, The undivided universe: an ontological interpretation of quantum theory, (Routledge, London) (1993).

[3] P. Holland, The Quantum Theory of Motion, An Account of the Broglie-Bohm Causal Interpretation of Quantum Mechanics, (Cambridge University Press, Cambridge) (1993).

[4] B. J. Hiley, Bohmian Non-commutative Dynamics: History and Developments, arXiv1303.6057 (2013).

[5] F. Sales Mayor, A. Askar, and H. Rabitz, Quantum fluid dynamics in the Lagrangian representation and applications to photodissociation problems, J. Chem. Phys. **111**, 2423(13) (1999).

[6] C. Lopreore and R. Wyatt, Quantum Wave Packet Dynamics with Trajectories, Phys. Rev. Lett. **82**, 5190–5193 (1999).

[7] A. S. Sanz, F. Borondo, and S. Miret-Artés, Causal trajectories description of atom diffraction by surfaces, Phys. Rev. B **61**, 7743–7751 (2000).

[8] Z. Wang, G. Darling, and S. Holloway, Dissociation dynamics from a de Broglie-Bohm perspective, J. Chem. Phys. **115**, 10373(9) (2001).

[9] R. Guantes, A. Sanz, J. Margalef-Roig, and S. Miret-Artés, Atom-surface diffraction: a trajectory description, Surface Science Reports **53**, 199–330 (2004).

[10] A. Sanz, B. Augstein, J. Wu, and C. Figueira de Morisson Faria, Alternative interpretation of high-order harmonic generation using Bohmian trajectories, arXiv:1205.529 (2012).

[11] R. Leacock and M. Padgett, Hamilton-Jacobi Theory and the Quantum Action Variable, Phys. Rev. Lett. **50**, 3–6 (1983).

[12] R. Leacock and M. Padgett, Hamilton-Jacobi/action-angle quantum mechanics, Phys. Rev. D **28**, 2491–2502 (1983).

[13] C. M. Bender and S. Boettcher, Real Spectra in Non-Hermitian Hamiltonians Having PT Symmetry, Phys. Rev. Lett. **80**, 5243–5246 (1998).

[14] C. M. Bender, Making sense of non-Hermitian Hamiltonians, Rept. Prog. Phys. **70**, 947–1018 (2007).

[15] A. Mostafazadeh, Pseudo-Hermitian Representation of Quantum Mechanics, Int. J. Geom. Meth. Mod. Phys. **7**, 1191–1306 (2010).

[16] A. Nanayakkara, Classical trajectories of 1D complex non-Hermitian Hamiltonian systems, J. Phys. **A37**, 4321–4334 (2004).

[17] C. M. Bender, D. D. Holm, and D. W. Hook, Complex Trajectories of a Simple Pendulum, J. Phys. **A40**, F81–F90 (2007).

[18] C. M. Bender, D. W. Hook, and K. S. Kooner, Classical Particle in a Complex Elliptic Potential, J. Phys. **A43**, 165201 (2010).

[19] C. M. Bender, D. D. Holm, and D. W. Hook, Complexified Dynamical Systems, J. Phys. **A40**, F793–F804 (2007).

[20] C. M. Bender, J. Feinberg, D. W. Hook, and D. J. Weir, Chaotic systems in complex phase space, Pramana J. Phys. **73**, 453–470 (2009).

[21] A. Fring, A note on the integrability of non-Hermitian extensions of Calogero-Moser-Sutherland models, Mod. Phys. Lett. **21**, 691–699 (2006).

[22] A. Fring and M. Znojil, $\mathcal{PT}$-Symmetric deformations of Calogero models, J. Phys. **A40**, 194010(17) (2008).

[23] P. E. G. Assis and A. Fring, From real fields to complex Calogero particles, J. Phys. **A42**, 425206(14) (2009).

[24] A. Fring and M. Smith, Antilinear deformations of Coxeter groups, an application to Calogero models, J. Phys. **A43**, 325201(28) (2010).

[25] C. M. Bender and T. Arpornthip, Conduction bands in classical periodic potentials, Pramana J. Phys. **73**, 259–268 (2009).

[26] A. Cavaglia, A. Fring, and B. Bagchi, PT-symmetry breaking in complex nonlinear wave equations and their deformations, J.Phys.A **A44**, 325201 (2011).

[27] A. Fring, PT-symmetric deformations of integrable models, Phil. Trans. Roy. Soc. Lond. **A371**, 20120046 (2013).

[28] J. Klauder, Quantization without quantization, Annals Phys. **237**, 147–160 (1995).

[29] J. Klauder, Coherent states for the hydrogen atom, J. Phys. **A29**, L293–L298 (1996).

[30] J.-P. Gazeau and J. R. Klauder, Coherent states for systems with discrete and continuous spectrum, J. Phys. A **32**, 123–132 (1999).

[31] J.-P. Antoine, J.-P. Gazeau, P. Monceau, J. R. Klauder, and K. A. Penson, Temporally stable coherent states for infinite well and Pöschl–Teller potentials, J. Math. Phys. **42**, 2349–2387 (2001).

[32] C.-D. Yang, Trajectory interpretation of the uncertainty principle in 1D systems using complex Bohmian mechanics, Phys.Lett. **A 372**, 6240–6253 (2008).

[33] Y. Goldfarb, I. Degani, and D. J. Tannor, Bohmian mechanics with complex action: A new trajectory-based formulation of quantum mechanics, J. Chem. Phys. **125**, 231103 (2006).

[34] C. Chou and R. E. Wyatt, Quantum trajectories in complex space, Phys. Rev. **A 76**, 012115 (2007).

[35] M. John, Probability and complex quantum trajectories, Annals of Physics **324**, 220–231 (2009).

[36] L. Mandel, Sub-Poissonian photon statistics in resonance fluorescence, Opt. Lett. **4**, 205–207 (1979).

[37] M. John, Modified de Broglie-Bohm approach to quantum mechanics, Found. Phys. Lett. **15**, 329–343 (2002).

[38] C.-D. Yang, Modeling quantum harmonic oscillator in complex domain, Chaos, Solitons and Fractals **30**, 342–362 (2006).

[39] G. Pöschl and E. Teller, Bemerkungen zur Quantenmechanik des anharmonischen Oszillators, Z. Phys. **83**, 143–151 (1933).

[40] H. Kleinert and I. Mustapic, Summing the spectral representations of Pöschl–Teller and Rosen-Morse fixed-energy amplitudes, J. Math. Phys. **33**, 643(20) (1992).

[41] M. John and K. Mathew, Coherent States and Modified de Broglie-Bohm Complex Quantum Trajectories, arXiv:1104.3197 (2011).

[42] S. Dey and A. Fring, Squeezed coherent states for noncommutative spaces with minimal length uncertainty relations, Phys. Rev. **D86**, 064038 (2012).

[43] S. Dey, A. Fring, L. Gouba, and P. G. Castro, Time-dependent $q$-deformed coherent states for generalized uncertainty relations, Phys. Rev. D **87**, 084033 (2013).